JOURNAL OF MATERIALS SCIENCE 25 (1990) 1690–1698

Synthesis and characterization of silicon nitride whiskers

MING-JONG WANG, HARUE WADA
Department of Materials Science and Engineering, The University of Michigan, Ann Arbor, Michigan 48109, USA

Silicon nitride whiskers were synthesized by the carbothermal reduction of silica under nitrogen gas flow. The formation of silicon nitride whiskers occurs through a gas-phase reaction, $3SiO(g) + 3CO(g) + 2N_2(g) = Si_3N_4(\beta) + 3CO_2(g)$, and the VS mechanism. The generation of SiO gas was enhanced by the application of a halide bath. Various nitrogen flow rates resulted in different whisker yields and morphologies. A suitable gas composition range of N_2, SiO and O_2 is necessary to make silicon nitride stable and grow in a whisker form. The oxygen partial pressure of the gas phase was measured by an oxygen sensor and the gas phase was analysed for CO/CO_2 by gas chromatography. Silicon nitride was first formed as a granule, typically a polycrystalline, and then grown as a single crystal whisker from the {1 0 0} plane of the granule along the ⟨2 1 0⟩ direction. The whiskers were identified as β'-sialon with Z value ranging from 0.8 to 1.1, determined by lattice parameter measurements.

1. Introduction

Ceramic whiskers, offering the advantages of high melting points, low densities and high moduli, have become important reinforcing materials in composites. The improving effects of ceramic whiskers on the mechanical properties of both ceramic-matrix composites [CMC] and metal-matrix composites [MMC] have been reported [1–4]. At present, silicon carbide whiskers are the most widely used and studied ceramic whiskers [1–6]. Since different matrices paired with different reinforcing materials would give specific advantages, other whiskers are expected to become the focus of studies as well. For instance, Si_3N_4(w)–Al composite has been reported [7] to be superior to SiC(w)–Al composite with a higher tensile strength and better machinability. In fact, silicon nitride, with good high temperature strength and thermal shock resistance, is likely to be one of the candidates of reinforcing materials for high temperature composites.

Unlike SiC whisker, studies on the Si_3N_4 whisker formation are very limited. Gribkov *et al.* [8] have formed α-Si_3N_4 whiskers from a mixture of SiO_2 and Si in a (N_2 + H_2) atmosphere. The observation of droplets at whisker tips was evidence that whisker growth occurred by the VLS mechanism. The droplets were identified as Al–Si or Fe–Si alloy. Hayashi *et al.* [9] have grown Si_3N_4 whiskers by the nitridation of the SiO_2–C–Na_3AlF_6 system. They reported that the whiskers contained about 85% β'-sialon and 15% α-Si_3N_4 under optimum conditions. The β'-sialon whiskers were 1 to 10 μm in diameter and up to 10 mm in length. The Z value of the β'-sialon whiskers was estimated as 1.8 to 2.0 from the lattice parameters measurements by X-ray diffraction. They concluded that the whisker growth was by the VLS mechanism based on the droplets found at the tips of β'-sialon whiskers. The droplets contained Si, Al, Na O and N.

One of the reasons which prevents ceramic whiskers from becoming a major reinforcing material of composites is cost. The main objective of this project is to develop a process which can synthesize ceramic whiskers in an economical way. This objective can be achieved by the following approaches: (1) using widely available silica and carbon as the low-cost materials, (2) developing a process that can synthesize either silicon nitride or silicon carbide whiskers with only minor changes in processing variables, and (3) applying an auxiliary bath to promote the reaction rate through an intimate contact between the two reactants.

The first approach is quite straightforward. Our earlier work [10], which involved a thermodynamic calculation to analyse the equilibria among the phases in the Si–C–N–O system, provided insights regarding the second approach. These results were applied as a guideline to synthesize Si_3N_4 and SiC whiskers selectively with the same process, only by changing the flowing gas [11]. The requirements of a suitable auxiliary bath for the third approach have been outlined in the same study [11]. The purpose of the present study is further to understand the formation mechanism of Si_3N_4 whiskers and their characteristics.

2. Experimental procedure

2.1. Whisker synthesis

About 3 g of silica, carbon and halide ($3NaF \cdot AlF_3$ or NaF) mixture with an atomic ratio of Si:C:Na = 1:3:1 was charged to a graphite tube inside a horizontal graphite reaction chamber, which was directly connected to a gas inlet at one end and an outlet at the

0022–2461/90 $03.00 + .12

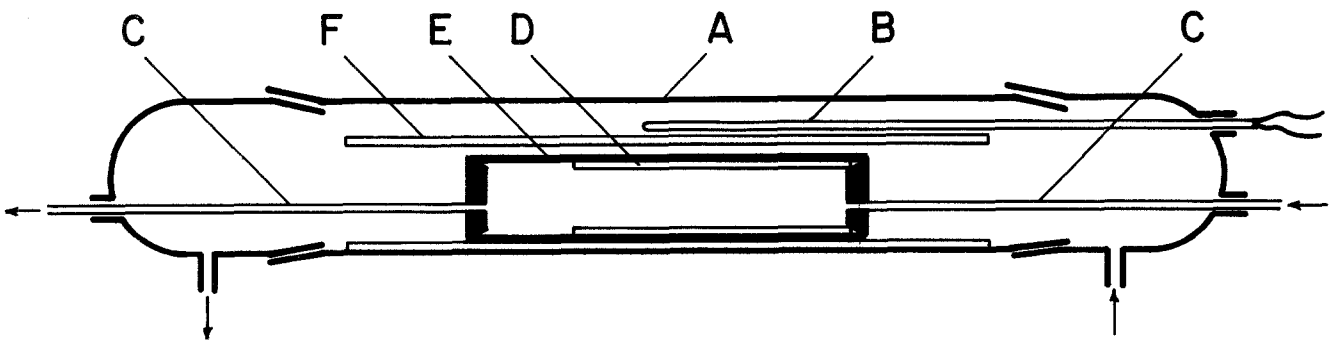

Figure 1 Schema of apparatus set-up. A, Mullite tube; B, thermocouple; C, gas inlet & outlet; D, graphite tube; E, graphite reaction tube; F, alumina protection tube.

other. The graphite reaction chamber was placed in a mullite tube. Fig. 1 shows a schema of the apparatus set-up.

A high purity (N_2 + 3% H_2) gas mixture was further purified through a $Mg(ClO_4)_2$ column, then introduced directly into the graphite reaction chamber. The gas flow rate was controlled by a Matheson 602 type flow meter, which had been calibrated by the bubble method. Four levels of flow rate were applied in this study: 25, 50, 75 and 100 cc min^{-1}.

All the reactions were carried out at 1623 K for 10 h. The temperature was measured by a Pt/Pt–10%Rh thermocouple. Upon the completion of reaction, the remaining carbon was oxidized in air at 973 K. For the purpose of comparisons, one run was carried out with pure Si instead of silica as the starting material. The reaction conditions and the associated results are summarized in Table I. The wt % of the whiskers grown at the upper part (see the next Section) was determined after the remaining carbon was oxidized.

2.2. Whisker characterization

The reaction products were identified by X-ray diffraction (XRD). Pure silicon was used as an internal standard to determine the lattice constants. The morphology and composition of whiskers were investigated by scanning electron microscope (SEM) and transmission electron microscope (TEM, Jeol 2000FX) microanalysis, respectively. Electron diffraction was applied to determine whisker growth direction.

2.3. Gas analysis

In selected runs, the oxygen partial pressure was measured continuously during the reaction by a $ZrO_2(CaO)$ solid electrolyte. The exhaust gas in these runs was also collected at certain time intervals for CO/CO_2 analysis by gas chromatography. The exhaust was led into a bubbler containing a saturated $PbCl_2$ solution. The fluorine in the exhaust was collected as PbClF precipitate.

2.4. Molten bath investigation

An additional experiment was performed to examine the nature of the molten bath. Identical starting materials were heated to 1373 K in a graphite crucible in air. Samples of the melt were taken and quenched on a copper plate at certain time intervals. Phases and composition of the sample were analysed by XRD and SEM/EDS, respectively, after the remaining carbon in the sample was oxidized in the same manner as mentioned previously.

3. Results and discussion

3.1. Whiskers

Whiskers were formed at the original powder bed and around the wall of the graphite tube. Fig. 2 shows a typical product collected from the powder bed before carbon burning. White wool-like whiskers had formed at *the upper part*, while *the lower part* was a mixture of short whiskers and powders containing approximately 40 wt % of carbon. The letter B shown in Fig. 2 indicates *the bottom area* of the wool-like whiskers.

Fig. 3 is a TEM micrograph of the whiskers grown at *the upper part*. These whiskers are transparent under an electron microscope, and identified by XRD as β'-sialon. The diameters of the whiskers are in a range from 0.5 to 1.2 μm, and the lengths are of the order of millimetres. The bottom part comprises short whiskers and powders, as shown in Fig. 4, and was identified by XRD as a mixture of β'-sialon and Si_2N_2O.

Fig. 5 shows a typical result of TEM microanalysis

TABLE I Summary of reaction conditions

No.	Starting materials	Halide	Flow rate, cc min^{-1}	Phase identification	
				Upper whiskers (wt %)	Lower mixture
1	SiO_2/C	$3NaFAlF_6$	25	β' (24.3)	β', SNO
2	SiO_2/C	$3NaFAlF_6$	50	β' (26.4)	β', SNO
3	SiO_2/C	$3NaFAlF_6$	75	β' (28.4)	β', SNO
4	SiO_2/C	$3NaFAlF_6$	100	β' (29.5)	β', SNO
5	SiO_2/C	NaF	50	α, β	SNO
6	Si/C	$3NaFAlF_6$	100	–	α, β, Si

β': β'-sialon, SNO: Si_2N_2O, α: α-Si_3N_4, β: β-Si_3N_4

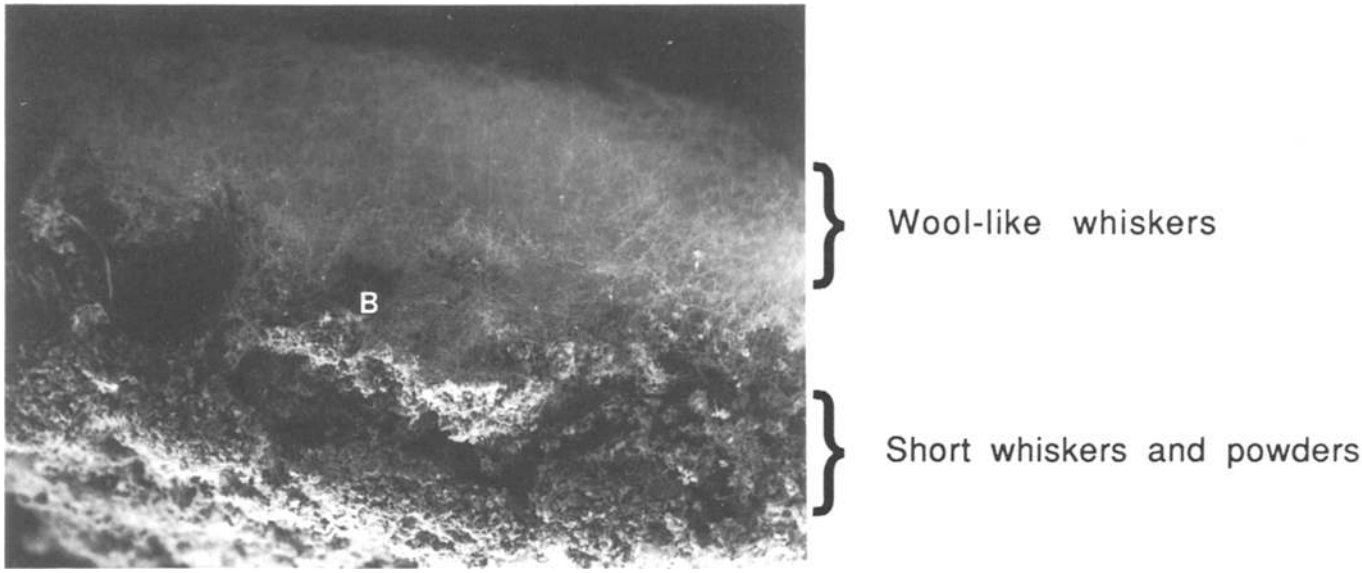

Figure 2 As-reacted product, before carbon burning, showing the wool-like whiskers at the upper part, the whiskers/powders mixture at the lower part and the bottom area of the wool-like whiskers indicated as the letter B.

of a β'-sialon whisker. The SiK_α and AlK_α peaks are clearly seen from the X-ray energy spectrum, while no sodium peaks were detected. The Si/Al ratio was determined by using the equation, $C_{Si}/C_{Al} = K_{Si-Al}I_{Si}/I_{Al}$, where C is element wt %, I is characteristic X-ray intensity and K is Cliff-Lorimer factor. A $K_{Si-Al} = 1.002$ was used in this study. Based on the measured Si/Al atomic ratio, the z value of β'-sialon ($Si_{6-z}Al_zO_zN_{8-z}$) was determined to be in the range from 0.8 to 1.1. The lattice parameters of β'-sialon are closely related to the z value, as demonstrated by Jack [12] and Hohnke and Tien [13]. Our results are in reasonable agreement with these studies.

Fig. 6 shows the whisker tip. Most of the whiskers have rectangular cross sections. The fact that no bulbs or droplets were ever observed at whisker tips suggests that the whisker growth was through the VS mechanism.

Efforts were made to investigate the roots of the whiskers. Typically, a polycrystalline was found at the root from which the whisker grew along the $\langle 2\,1\,0 \rangle$ direction, shown as Fig. 7. Fig. 8 reveals a relatively rare case in which a whisker stemmed from a single crystal. Both the whisker and the single crystal root have the same orientation, with $\langle 2\,1\,0 \rangle$ as the growth direction. It can be concluded that Si_3N_4 was first formed as a granule (either polycrystalline or single crystal), and then grew in a whisker form from the $\{1\,0\,0\}$ plane of the granule along the $\langle 2\,1\,0 \rangle$ direction.

With [3NaF·AiF_3] as the molten bath, β'-sialon was the main product; however, when [NAF] substituted for [3NaF·AlF_3], α-Si_3N_4 became the dominant phase. The α-Si_3N_4 whisker is easily distinguished by the ribbon-like morphology, as shown in Fig. 9, with about 1 μm in width and less than 0.1 μm in thickness. The growth direction of the α-Si_3N_4 whisker is

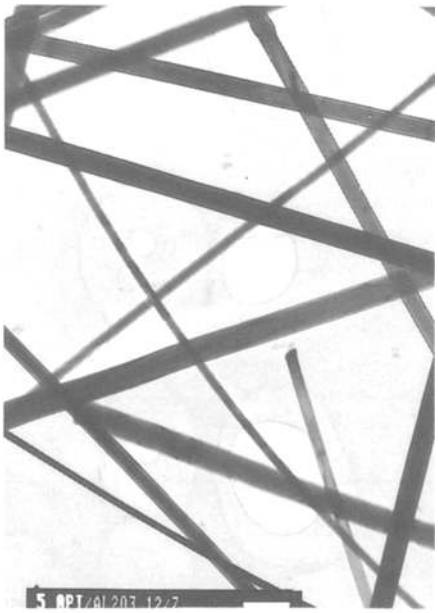

Figure 3 TEM micrograph of β'-sialon whiskers from the upper part (bar = 1 μm).

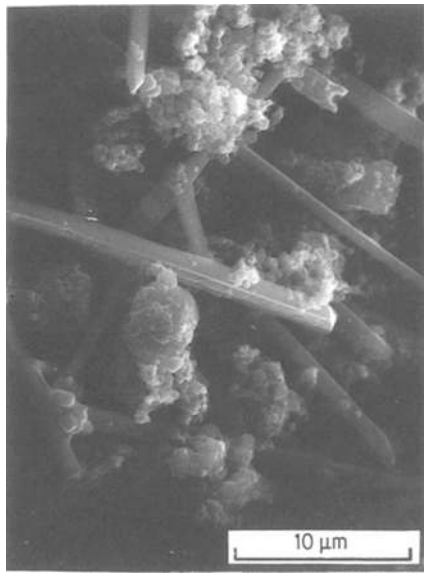

Figure 4 SEM micrograph of the lower part showing a mixture of whiskers and powders.

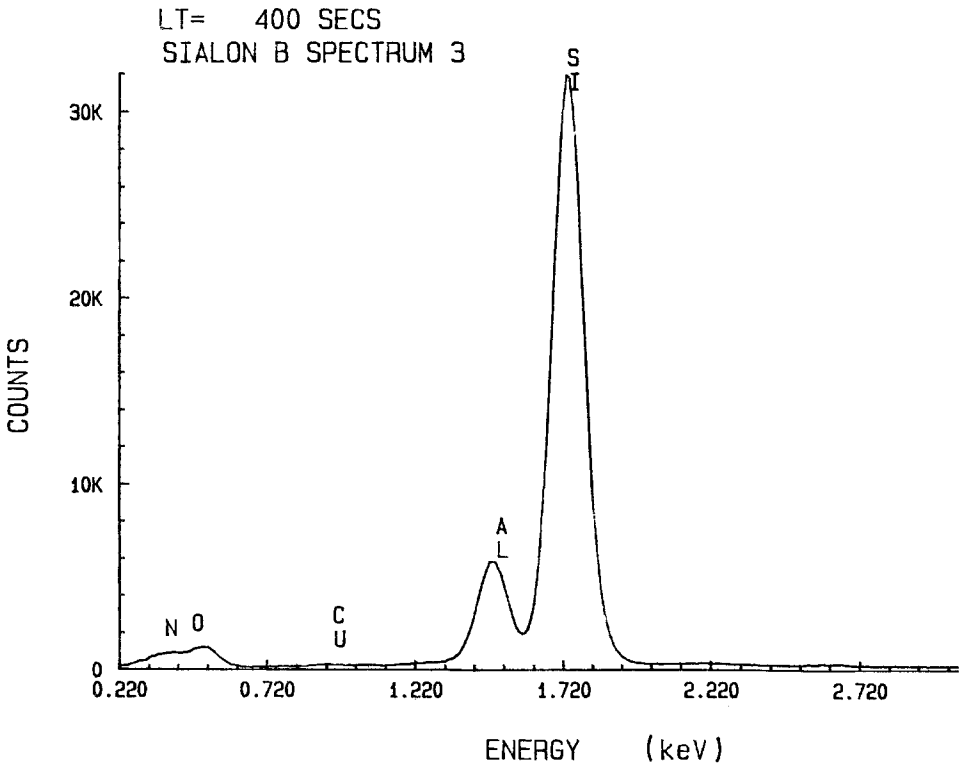

Figure 5 Typical X-ray energy spectrum of a β'-sialon whisker.

⟨2 1 1⟩. The same morphology of α-Si_3N_4 whiskers was also reported by other studies [8, 14].

3.2. Gas phase

The equilibrium partial pressure of oxygen was measured by a ZrO_2 sensor. The galvanic cell with a ZrO_2–(15 mol % CaO) solid electrolyte can be denoted as

$$Mo/O_2(Mo\text{–}MoO_2)/ZrO_2(CaO)/O_2(\text{in reaction})/Mo$$

The detailed structure of the ZrO_2 electrolyte and a method to determine the oxygen partial pressure can be found in [15] and [11].

Typically, the measured values of p_{O_2} were about 10^{-22} atm throughout the reaction period. Referring to the stability diagram (Fig. 8 in ref [10]), a $p_{O_2} = 10^{-22}$ atm is within the stable region of Si_3N_4 at $a_C = 1$, $p_{N_2} = 1$ atm and $T = 1623$ K.

The equilibrium p_{CO} was calculated from the measured p_{O_2} for $a_C = 1$ based on the following reaction,

$$C(s) + 1/2\ O_2(g) = CO(g) \qquad (1)$$

The measured p_{CO} and p_{CO_2} and the calculated p_{CO} are summarized in Table II. Taking into consideration the fact that the exhaust gas was collected at a much lower temperature, the agreement between the two values is reasonable. It indicates that p_{O_2} and p_{CO} were very close to their equilibrium values during the reaction. The CO_2 content in the exhaust was always below the analytical limit of 0.025 vol %. The equilibrium p_{CO_2} calculated at 1623 K and $a_C = 1$ for the following reaction is also lower than the analytical limit.

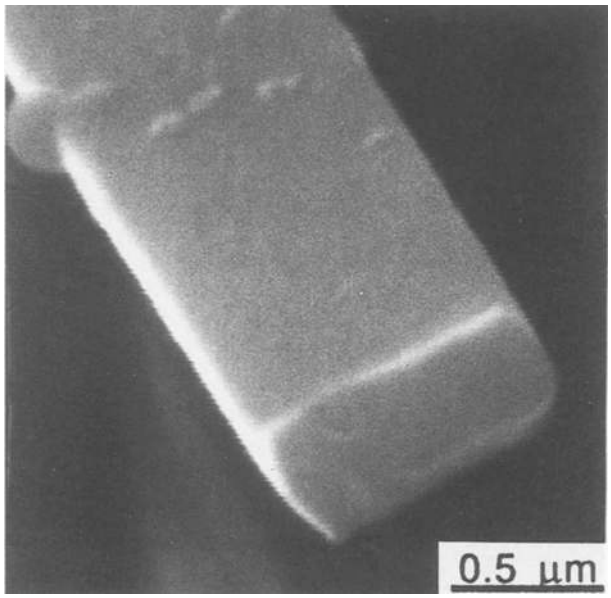

Figure 6 SEM micrograph of β'-sialon whisker showing a rectangular cross section.

Figure 7 SEM micrograph showing a polycrystalline granule at the root of a β'-sialon whisker.

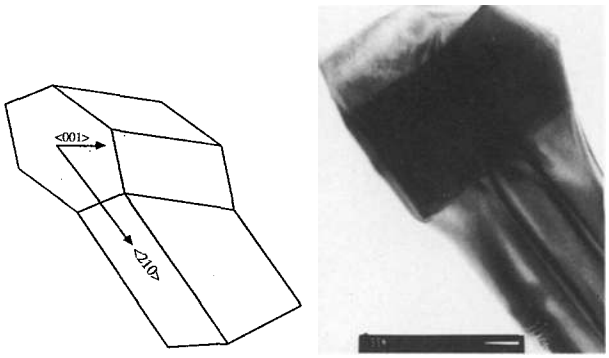

Figure 8 TEM micrograph of a β'-sialon whisker originated from a single crystal and an illustration of the whisker growth direction (bar = 100 nm).

$$CO_2(g) + C(S) = 2CO(g) \quad (2)$$

Therefore, it can be concluded that CO/CO_2 were also in equilibrium. Since the value of the equilibrium constant of the CO/CO_2 reaction is high ($K_2 = 3.68 \times 10^3$ at 1623 K), the effect of p_{CO_2} on whisker formation would be minimal when $a_C = 1$.

3.3. Molten bath

Fig. 10 shows a SEM micograph of the quenched molten [$3NaF \cdot AlF_3$] bath, with a Si X-ray map. The spherical morphology suggests that the molten bath had high surface tension and might have formed as molten droplets during the reaction. The uniform distribution of Si indicates that silica has dissolved into the molten bath. Although the phase diagram of the SiO_2–NaF–AlF_3 system is not available, it is well established that [Na_3AlF_6] forms low melting-point liquids with several other metallic oxides [16]. Saito *et al.* [17] have suggested that the addition of NaF, CaF_2 and Na_3AlF_6 to SiO_2 forms fluorosilicate melts at 1623 K. It is likely that the molten halide bath became Na–Al fluorosilicate as silica dissolved.

Low viscosity is one of the important factors in selecting a suitable auxiliary bath, since it is anticipated to affect the contact between silica and carbon as well as the gas evolution. The addition of fluoride is well known for reducing the viscosity of oxide melts [18, 19]. To evaluate the effect of the halide bath on the reaction between silica and carbon, carbon consumptions by the carbothermal reduction of silica were compared for the cases with and without the halide bath. Only 8% of the charged carbon was consumed when the bath was not applied, whereas the consumed carbon was about 35% in the presence of the halide bath. The carbothermal reduction of silica is expressed as:

$$SiO_2(s/l) + C(s) = SiO(g) + CO(g) \quad (3)$$

TABLE II CO/CO_2 Composition of the exhaust gas

Sample no	Collecting time*, min	CO vol %	CO_2 vol %	Calculated p_{CO}, atm
1	10	2.00	< 0.025	0.029
2	180	2.83	< 0.025	0.021
3	480	1.80	< 0.025	0.037

*Time after the reaction temperature reached 1623 K.

Figure 9 SEM micrograph of α-Si_3N_4 whiskers with NaF as molten bath.

The intimate contact between silica and carbon through the liquid phase resulted in the higher consumption rate of carbon. The evolution of SiO and CO gases from the spherical and low-viscosity molten droplets might have been assisted by the evolution of other gases, such as fluorine and fluorides. The crater-like openings on the surface of the quenched sample as seen in Fig. 10 may be evidence of gas evolution. The findings of [NaF] and [$3NaF \cdot AlF_3$] by XRD in the vaporized/condensed deposit at low-temperature area of the gas outlet confirmed the evolution of fluoride gases.

The pH value of the saturated $PbCl_2$ solution was changed as the exhaust was led into the bubbler, through the following reaction,

$$PbCl_2 + F^- = PbClF(s) + Cl^- \quad (4)$$

The pH value started to drop abruptly as the temperature approached the melting point of [$3NaF \cdot AlF_3$], 1282 K, and levelled off within 30 minutes. This fact implies that fluorine and fluorides started to evaporate at a very high rate during the early stages of melting, then the evaporation reduced until a steady rate was reached. Both the dissolution of silica into the melt and the initial evaporation of fluorine and fluorides from the melt could increase the viscosity of the melt and reduce the subsequent evaporation rate of fluorine and fluorides.

The quenched molten bath was identified as a mixture of [NaF] and [$3NaF \cdot AlF_3$] by XRD. The relative amount of [NaF] increased with increasing holding time. Thus the composition of the molten bath has shifted from [Na_3AlF_6] toward the [NaF]-rich end, referring to the NaF-AlF_3 phase diagram [20], which is in agreement with the fact that [AlF_3] has a higher vapour pressure than [NaF].

3.4. Reaction mechanism

3.4.1. Silicon nitride

As discussed previously, the whisker formation is likely through the VS mechanism. There are three possible reaction routes that could be responsible for the Si_3N_4

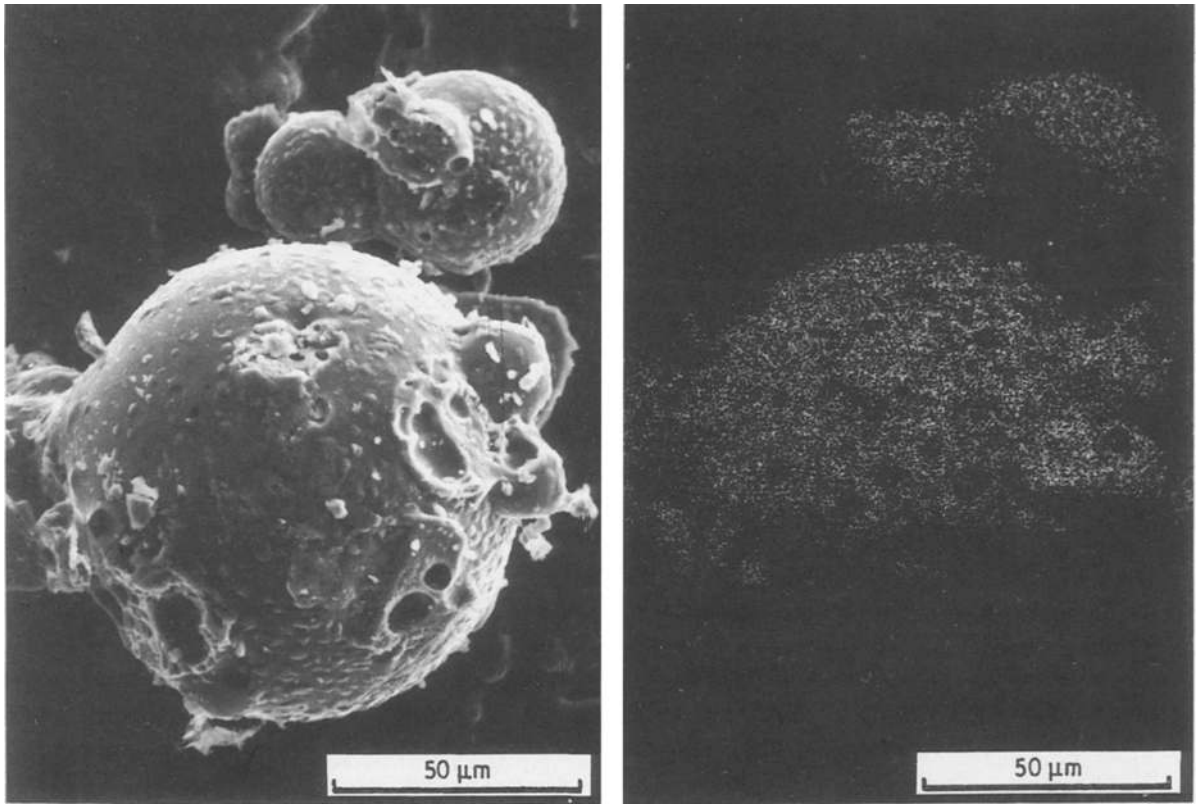

Figure 10 SEM micrograph of quenched halide bath and the X-ray map of Si.

whisker formation:

$$3SiO(g) + 3CO(g) + 2N_2(g) = Si_3N_4(\beta) + 3CO_2(g) \quad (5)$$

$$\Delta G^\circ_5 = -1437.972 + 0.942T, \quad kJ\,mol^{-1} \text{ of } Si_3N_4 \quad (5\text{-}1)$$

$$3SiO(g) + 3C(s) + 2N_2(g) = Si_3N_4(\beta) + 3CO(g) \quad (6)$$

$$\Delta G^\circ_6 = -952.356 + 0.438T, \quad kJ\,mol^{-1} \text{ of } Si_3N_4 \quad (6\text{-}1)$$

$$3SiF_4(g) + 2N_2(g) = Si_3N_4(\beta) + 6F_2(g) \quad (7)$$

$$\Delta G^\circ_7 = 3920.19 + 0.018T, \quad kJ\,mol^{-1} \text{ of } Si_3N_4 \quad (7\text{-}1)$$

All the standard free energies of formation used in this study were obtained from JANAF Tables [21], except that of $Si_3N_4(\beta)$ and $Si_2N_2O(s)$, which were from the same source as described in [10]. The contribution from Equation (7) is considered to be insignificant for the following reasons: (1) the free energy change of Equation (7) is 3949 kJ at 1623 K which is much higher than those of Equation (5) and (6), 91 kJ and −241 kJ, respectively, and (2) the fluorine recovery as the PbClF precipitate was always about 40% despite the fact that the Si yield changed as reaction conditions were changed. However, the evolution of $SiF_4(g)$ from the melt may enhance the evolution of SiO(g). The necessary presence of solid carbon at the reaction site, i.e., the whisker tip, rules out the possibility of the gas–solid reaction of Equation (6) as the major reaction, especially when the whiskers were as long as millimetres; furthermore, Si_3N_4 whiskers have been found on an alumina substrate where solid carbon is absent. Therefore, Equation (5) is the most probable reaction for the Si_3N_4 whisker formation.

The importance of SiO gas for Si_3N_4 whisker formation was clearly demonstrated by replacing SiO_2 with Si as the starting material (No. 6 in Table I): no whiskers were formed and the carbon consumption was only one-fourth of that in the SiO_2 cases of the same reaction conditions. The major morphology of the product was the hexagonal particulate, as shown in Fig. 11. X-ray diffraction indicated that the product was a mixture of α-, β-Si_3N_4 and about 40 wt % of Si. The remaining Si was identified as the unreacted starting Si from the partially changed morphology.

For the crystal grown from the vapour phase, it is generally believed that the growth form is closely related to the supersaturation ratio [22], which is a combination of the concentrations of the reactant gases. In general, a lower supersaturation ratio favours the formation of whiskers, whereas a higher supersaturation would result in powders. Since the gas-phase reaction of Equation (5) is the route for Si_3N_4 formation, the growth form of Si_3N_4 is closely related to the partial pressures of N_2, SiO and CO/CO_2.

The relative amount of the wool-like whiskers (the upper part) increases with increasing the nitrogen flow rate, as summarized in Table I. One of the effects of an increasing flow rate is a larger supply of nitrogen gas to the reaction zone. However, a higher flow rate could also change the partial pressures of SiO(g) and CO(g) at the reaction zone and result in a supersaturation ratio suitable for the formation of Si_3N_4 in whisker form.

Fig. 12 is a close-up of the bottom area of the wool-like whiskers (area B in Fig. 2). It is clear that

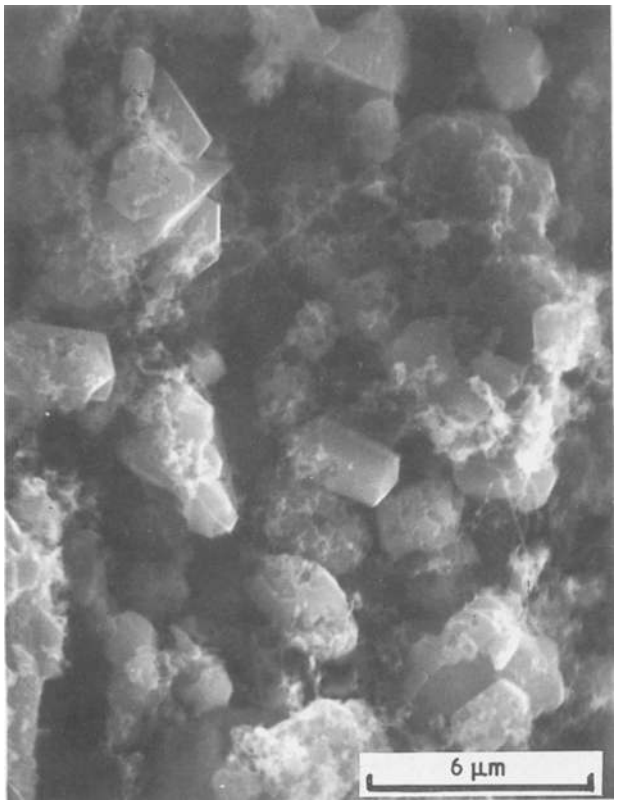

Figure 11 SEM micrograph of the product with Si as starting material.

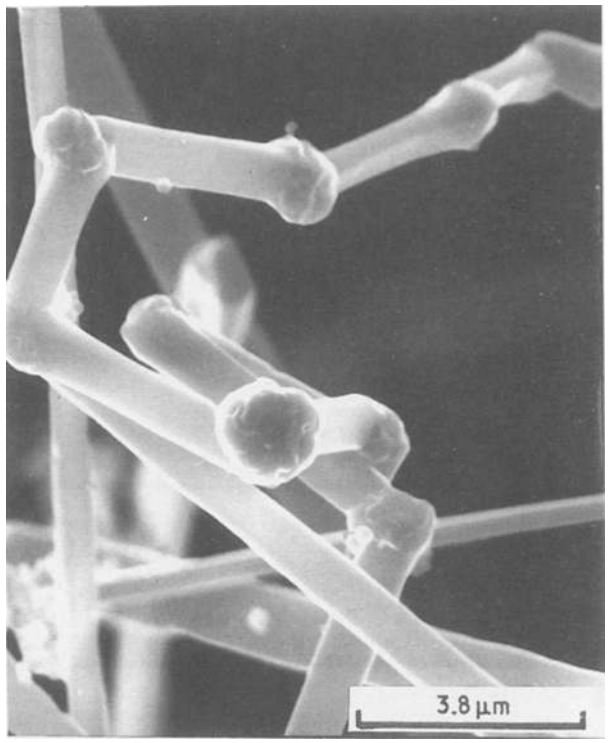

Figure 12 SEM micrograph showing whiskers with knuckles from the bottom area of the wool-like whiskers.

some of the whiskers in this area have "knuckles" which formed during their growth. SEM/EDX showed that both whiskers and knuckles have the same β'-sialon composition. Most of the knuckles were identified as polycrystalline by electron diffraction, while the whisker portions between knuckles were single crystals. It seems that the anisotropic whisker growth and the isotropic polycrystalline growth have occurred alternately in these particular whiskers. From the fact that these whiskers were only found at the bottom area of the wool-like whiskers, it suggests that the formation of these whiskers is location-related. Even though it is not yet clear how the nitrogen gas reaches the bottom area (e.g. by physically flowing or dissolving into the melt), the supply of nitrogen to this area would not be as easy as to the upper area. Deeper in the powder bed (the lower part), the nitrogen supply could even be less sufficient. As a result, the gas composition is expected to fluctuate during the formation of whiskers in the bottom area. The changing gas composition around the growing whisker in the bottom area probably is responsible for the change of growth form, i.e. from whisker to knuckle and vice versa. The even less sufficient supply of nitrogen in the lower part might result in a supersaturation ratio which made Si_3N_4 in powder form.

The formation of β'-sialon can be expressed as the following reaction,

$$(6 - z)SiO(g) + (4 - z/2)N_2(g) + (6 - 2z)CO(g) + zAl(g) = Si_{(6-z)}Al_zO_zN_{(8-z)} + (6 - 2z)CO_2(g) \quad (8)$$

Because aluminium and oxygen substitute for silicon and nitrogen, respectively, in forming β'-sialon, the oxygen partial pressure in the gas phase is expected to become lower. The presence of aluminium seems to stabilize the β-type structure by (1) forming β'-sialon that is β-type, and (2) dissolving oxygen into β'-sialon and hence reduces p_{O_2} in the gas phase. The β-type is known to be more stable than the α-type at lower p_{O_2}. In the absence of aluminium, both α- and β-type would grow competitively, depending on the temperature and p_{O_2}. This may explain the observation of α-Si_3N_4 whiskers when NaF was used as the halide bath (No. 5 in Table I).

3.4.2. Silicon oxynitride

Si_2N_2O was found at the lower part along with Si_3N_4, even though the oxygen partial pressure was low enough to suppress its formation. A thermodynamic calculation was carried out to futher analyse the effects of gas composition, including SiO(g), on the stability of phases in the Si–C–N–O system.

In the Si–C–N–O system, the formations of solid phases from the major gas phase components can be expressed as follows:

$$3SiO(g) + 3C(s) + 2N_2(g) = Si_3N_4(\beta) + 3CO(g) \quad (9)$$

$$\log K_9 = \log a_{Si_3N_4} + 3\log p_{CO} - 3\log p_{SiO} - 3\log a_C - 2\log p_{N_2} = 49747/T - 22.8 \quad (9\text{-}1)$$

$$2SiO(g) + C(s) + N_2(g) = Si_2N_2O(s) + CO(g) \quad (10)$$

$$\log K_{10} = \log a_{Si_2N_2O} + \log p_{CO} - 2\log p_{SiO} - \log a_C - \log p_{N_2} = 29211/T - 10.81 \quad (10\text{-}1)$$

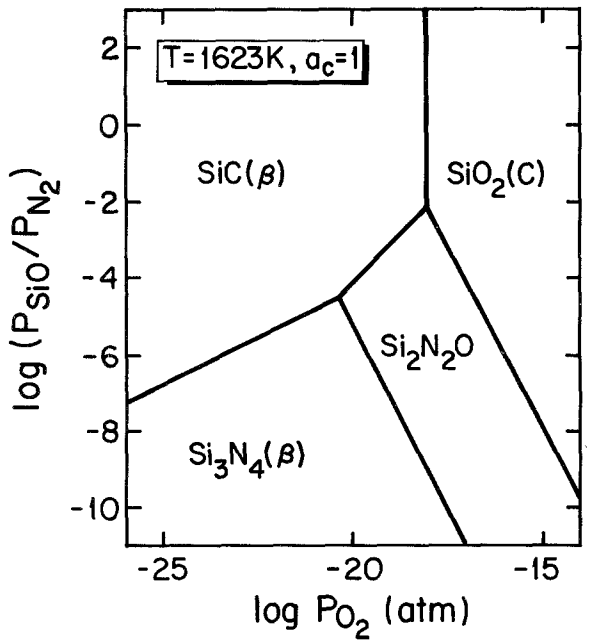

Figure 13 Phase stability diagram as a function of p_{O_2} and p_{SiO}/p_{N_2} at $T = 1623\,K$ and $a_C = 1$.

$$SiO(g) + 2C(s) = SiC(\beta) + CO(g) \quad (11)$$

$$\log K_{11} = \log a_{SiC} + \log p_{CO} - \log p_{SiO} - 2\log a_C$$
$$= 4277/T - 0.16 \quad (11\text{-}1)$$

$$SiO(g) + CO(g) = SiO_2(c) + C(s) \quad (12)$$

$$\log K_{12} = \log a_{SiO_2} + \log a_C - \log p_{SiO} - \log p_{CO}$$
$$= 35261/T - 17.50 \quad (12\text{-}1)$$

The partial pressures of SiO(g), N_2(g) and CO(g) for each equilibrium were determined by solving the related two equations; for instance, Equations 9-1 and 10-1 were solved simultaneously at given conditions for the Si_3N_4/Si_2N_2O equilibrium. Since solid Si_3N_4 and Si_2N_2O were in equilibrium, $a_{Si_3N_4} = a_{Si_2N_2O} = 1$. If $a_C = 1$ (referred to graphite) and $p_{CO} = 10^{-2}$ atm, then p_{SiO} and p_{N_2} were calculated as 2.57×10^{-5} atm and 1 atm respectively, at $T = 1623\,K$. The same principle was applied to other equilibria. For the purpose of comparisons with the established stability diagrams [10], the p_{CO} values were converted to p_{O_2} based on the equilibrium of Equation 1. A stability diagram which shows the relationship between the gas phase composition and the stable solid phases was constructed as a function of p_{O_2} and (p_{SiO}/p_{N_2}) ratio, as shown in Fig. 13. The corresponding p_{N_2} and p_{O_2} at each invariant point are consistent with the values determined previously [10].

Each boundary in Fig. 13 represents the equilibrium p_{O_2} and (p_{SiO}/p_{N_2}) of the corresponding two solid phases at 1623 K. Considering the equilibrium between $Si_3N_4(\beta)$ and Si_2N_2O, there is a specific (p_{SiO}/p_{N_2}) ratio at a given p_{O_2}. If the (p_{SiO}/p_{N_2}) ratio of a gas phase is higher than the specific value for the given p_{O_2}, Si_2N_2O is the stable phase, whereas $Si_3N_4(\beta)$ becomes stable if the (p_{SiO}/p_{N_2}) ratio is lower than the specific value. The (p_{SiO}/p_{N_2}) ratio at *the lower part* might be considerably higher than at *the upper part*, because there might not be a sufficient supply of nitrogen gas to the lower part of the melt and the generated SiO gas might not leave freely. It could be concluded that the localized high (p_{SiO}/p_{N_2}) ratio was responsible for the formation of Si_2N_2O at the lower part, even under the very low oxygen partial pressure in the gas phase.

4. Summary

(1) The formation of Si_3N_4 and β'-sialon whiskers occurs through a gas-phase reaction involving SiO(g), and VS mechanism.
(2) β'-sialon was first formed as a granule, typically a polycrystalline, and then grown as a single crystal whisker from the {1 0 0} plane of the granule along the ⟨2 1 0⟩ direction.
(3) β'-sialon whiskers, with about 0.7 μm diameter and $z = 0.8$ to 1.1, are synthesized by the present process.
(4) The application of a halide bath enhances the generation of SiO gas by dissolving the silica into the bath.
(5) The rate of supply of N_2 gas is a critical factor not only for determining the growth of Si_3N_4 but also for the formation of Si_2N_2O.
(6) The presence of Al stabilizes the β-type structure by forming β'-sialon and subsequently reducing p_{O_2} in the system.

Acknowledgement

This research is supported by NSF through MSM-8719951.

References

1. P. F. BECHER and G. C. WEI, *J. Amer. Ceram. Soc.* **67** (1984) C-267.
2. S. T. BULJAN, J. G. BALDONI and M. L. HUCKABEE, *Amer. Ceram. Soc. Bull.* **66** (1987) 347.
3. D. F. HASSON, S. M. HOOVER and C. R. CROWE, *J. Mater. Sci.* **20** (1985) 4147.
4. S. V. NAIR, T. K. TIEN and R. C. BATES, *Int. Met. Rev.* **30** (1985) 275.
5. G. A. BOOTSMA, W. F. KNIPPENBERG and G. VERSPUI, *J. Cryst. Growth* **11** (1971) 297.
6. J. V. MILEWSKI, F. D. GAC, J. J. PETROVIC and S. R. SKAGGS, *J. Mater. Sci.* **20** (1985) 1160.
7. M. MATSUBARA, Y. NISHIDA, M. YAMADA, I. SHIRAYANAGI and T. IMAI, *J. Mater. Sci. Lett.* **6** (1987) 1313.
8. V. N. GRIBKOV, V. A. SILAEV, B. V. SCHETANOV, E. L. UMANTSEV and A. S. ISAIKIN, *Soviet Physics-Crystallography* **16** (1972) 852.
9. T. HAYASHI, S. KAWABE and H. SAITO, *Yogyo-kyokai-shi* **94** (1986) 19.
10. H. WADA, M-J. WANG and T. Y. TIEN, *J. Amer. Ceram. Soc.* **71** (1988) 837.
11. H. WADA and M-J. WANG, in Proceedings of International Conference on Whisker- and Fibre-Toughened Ceramics, Oak Ridge, USA, June 1988, edited by R. A. Bradley *et al.* (ASM International, 1988) p. 63.
12. K. H. JACK, *J. Mater. Sci.* **11** (1976) 1135.
13. H. HOHNKE and T. Y. TIEN, in "Progress in Nitrogen Ceramics", edited by F. L. Riely (Martinus Nijhoff Publishers, 1983) p. 101.
14. A. SZWEDA, A. HENDRY and K. H. JACK, in "Special Ceramics", Vol. 7, edited by J. Taylor and P. Popper (British Ceramics Society, Stoke-on Trent, 1981) p. 107.
15. T. MURAYAMA and H. WADA, in Proceedings of the 2nd International Symposium on Metallurgical Slags and Fluxes, Lake Tahoe, USA, November 1984, edited by H. A. Fine and D. R. Gaskell (Metall. Soc. AIME, 1984) p. 135.

16. "Phase Diagrams for Ceramics", Vol. I (The American Ceramic Society, Inc.) p. 475.
17. H. SAITO, T. HAYASHI and K. MIURA, *Nippon Kagaku Kaishi* (1982) 401.
18. P. M. BILLS, *J. Iron Steel Inst.* **200** (1963) 133.
19. M. KATO and S. MINOWA, *Trans. ISIJ* **9** (1969) 31.
20. "Phase Diagrams for Ceramics", Vol. V (The American Ceramic Society, Inc.) p. 83.
21. JANAF Thermochemical Tables, 3rd ed., (American Chemical Society and American Institute of Physics for National Bureau of Standards, 1986).
22. W. B. CAMPBELL, in "Whisker Technology", edited by A. P. Levitt (Wiley, New York, 1970) p. 37.

Received 1 November 1988
and accepted 12 April 1989